Interferometric Strain Measurements with a Fiber-Optic Probe

Introduction

Experience with spherical cryogenic targets at the Laboratory for Laser Energetics (LLE) has led to the conclusion that mechanical vibrations of National Ignition Facility (NIF)–scale cryogenic direct-drive targets must be anticipated and mitigated in order to achieve the required implosion quality. Controlling the target position and isolating vibration sources with a closed-loop control system require a target position metrology system and an actuator for active vibration compensation. The chief concern with closed-loop control is the limitation placed on the metrology system because of the unique inertial confinement fusion (ICF) experimental environment at the NIF. At LLE, high-speed cameras mounted on the target chamber walls are used to track the location of ICF targets. At the NIF, mounting locations for a similar target tracking system cannot be guaranteed, so an alternative target position sensor must be designed. The sensor must be able to operate in high vacuum at cryogenic temperatures without interfering with diagnostics, beam paths, or general functioning of NIF cryogenic direct-drive targets. This article proposes to integrate the sensor into the target assembly. Lastly, the nature of ICF experiments means that any sensor close to the target will be destroyed after every experiment, so the sensor must be easily replaceable and economical.

A strain-based target position metrology system is presented here. By measuring the strain on the target support stalk, the position of the target stalk's tip can be calculated with solid mechanics, i.e., Euler–Bernoulli beam theory. Using geometry and dynamic models, the position of the target stalk's tip can then be related to the target capsule's position. A small fiber-based strain gauge will make it possible to deliver the strain sensor within the target package assembly.

Strain measurements are important for monitoring many engineering applications, such as strain in bridges to predict failure and structural health. Many different strain-measurement techniques are available, such as mechanical-strain gauges, resistive-strain gauges, piezoelectric elements,[1] capacitive-strain gauges, vibration-based strain gauges, and fiber Bragg gratings (FBG's),[2] among other more-specialized applications.[3] Choosing the most-appropriate sensor is driven mainly by cost, environment, and required resolution. ICF experimental results deteriorate for target motions of more than 10 μm of target displacement relative to the beam focus. Based on this, a 1-μm target displacement resolution becomes the design goal, which is equivalent to $\leq$2-$\mu\epsilon$ resolution at the base of the hollow support stalk. In addition, for use in a closed-loop control positioning system, the metrology system's sampling rate must be at least 1 kHz in order to exceed the Nyquist frequency determined by the first natural frequency of the target and its support structure.

In 1978, Butter and Hocker[4] developed a single-mode optical-fiber strain metrology system, although the system was limited by manual fringe counting and fiber management. The research presented here expands on this work by developing a novel fiber-optic heterodyne interferometer and a single-mode (SM) optical-fiber strain probe. The SM fiber probe is bonded to the target support stalk and is subjected to strain as the target is displaced. As the optical path length (OPL) of the measurement arm of the interferometer changes because of applied strain, the interferometer measures the resulting phase shift. The measured phase shift can then be used to calculate target position in a closed-loop control setup. The system also allows for remote sensing, so that the interferometer itself can be located in a thermally stable, vibration-isolated environment with an optical-fiber link between the probe and the interferometer. The new probe is economical, has high resolution and range when coupled with the fiber-optic heterodyne interferometer, and is compatible with the high-vacuum, cryogenic environment found in the target chamber. Finally, the interferometer can be linked to length standards of the National Institute of Standards and Technology by using a frequency-stabilized laser source for full traceability of any measurements. The following theory relates the strain applied to the single-mode fiber and the measured OPL change.

Mathematical Theory

To measure target position with a strain sensor, the relation between the applied strain and the resulting OPL change must be derived. A simple experimental setup uses a sensor bonded to a cantilevered beam. With this mathematical framework, the measured OPL change in a fiber strain gauge can be correlated to the cantilevered beam-tip displacement. The OPL of a beam of light is equal to

$$L_o = nL, \tag{1}$$

where n is the effective index of refraction of the material and L is the physical path length. The change in the optical path length in optical fiber, in response to an applied strain and temperature change, is

$$\Delta L_o = n\Delta L + L\Delta n, \tag{2}$$

where ΔL and Δn are given by

$$\begin{aligned} \Delta L &= \frac{\partial L}{\partial l}\Delta l + \frac{\partial L}{\partial T}\Delta T = \epsilon L + \alpha L \Delta T, \\ \Delta n &= \frac{\partial n}{\partial l}\Delta l + \frac{\partial n}{\partial T}\Delta T = -p_e n\epsilon + \zeta n \Delta T, \end{aligned} \tag{3}$$

where ϵ is the applied strain, ΔT is an applied temperature change, α is the coefficient of linear expansion for the material, $p_e = n^2\left[p_{12} - \nu\left(p_{11} + p_{12}\right)\right]/2$ is the effective strain-optic coefficient,[5] and ζ is the temperature-optic coefficient. Substituting Eq. (3) into Eq. (2) the OPL change becomes

$$\Delta L_o = L_o\left[\epsilon\left(1-p_e\right) + \Delta T\left(\alpha + \zeta\right)\right], \tag{4}$$

where $L_o = nL$ is the original optical path length. If there are nonuniform strains, the OPL change is written as

$$\Delta L_o = n\left(1-p_e\right)\int_{x_1}^{x_2} \epsilon \mathrm{d}x + \Delta T n L\left(\alpha + \zeta\right), \tag{5}$$

where x_1 and x_2 are the start and end points of the probe (seen in Fig. 144.24). If the fiber is isotropic and linear elastic and has a large length-to-width ratio, the Euler–Bernoulli beam theory applies and the strain at a longitudinal position x is given by

$$\epsilon = \frac{Mc}{EI} = \frac{F(L-x)c}{EI}, \tag{6}$$

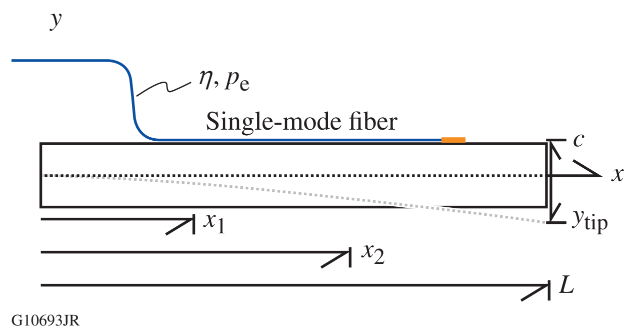

Figure 144.24
Schematic of the experimental test cantilever.

where F is the end applied force, L is the original length of the substrate, c is the transverse location of interest measured from the neutral axis, E is the elastic modulus of the fiber, and I is the second moment of area of the system. The displacement of the beam's tip can be related to the applied force with a one-degree-of-freedom spring approximation

$$F = \frac{3EI}{L^3} y_{\mathrm{tip}}, \tag{7}$$

where F is the end applied force. Equation (7) applies only to a cantilevered substrate, and an alternate relation is required for differing boundary conditions. Combining Eqs. (5)–(7), the OPL change becomes

$$\Delta L_o = \frac{3cny_{\mathrm{tip}}\left(1-p_e\right)}{L^3}\int_{x_1}^{x_2}(L-x)\,\mathrm{d}x + \Delta T n L\left(\alpha + \zeta\right), \tag{8}$$

which relates the tip displacement of a substrate cantilever and a temperature change to an OPL variation in a fiber probe bonded to the surface of a cantilevered substrate.

Now that we have a relation between a measured change in the optical path length and the tip displacement [Eq. (8)], the OPL change must be related to the phase shift measured with the heterodyne interferometer. A phase change measured with a heterodyne interferometer is related to the OPL change by

$$\Delta\phi = \frac{2\pi N \Delta L_o}{\lambda}, \tag{9}$$

where $\Delta\phi$ is the phase shift and λ is the wavelength of the light in use.[6] Substituting Eq. (8) into Eq. (9),

$$\Delta\phi = \frac{2\pi N}{\lambda}\left[\frac{3cny_{\text{tip}}(1-p_{\text{e}})}{L^3}\right.$$

$$\left.\times \int_{x_1}^{x_2} (L-x)\,\mathrm{d}x + \Delta TnL(\alpha+\zeta)\right], \tag{10}$$

allows one to calculate the target position by measuring a phase shift with a heterodyne interferometer. The optically measured tip displacement used in this work is

$$y_{\text{opt}} = \left(\frac{\Delta\phi\lambda L^3}{2\pi N}\right)\left[3cn(1-p_{\text{e}})\int_{x_1}^{x_2}(L-x)\,\mathrm{d}x\right]^{-1}, \tag{11}$$

which is Eq. (10) rearranged with ΔT assumed to be negligible. The equivalent of Eq. (11) for the resistive-strain gauge is

$$y_{\text{res}} = \frac{\epsilon L^3}{3c(L-x_3)}, \tag{12}$$

where ϵ is the measured strain and x_3 is the location of the center of the strain gauge. The geometric and optical parameters in Eqs. (11) and (12) are listed in Table 144.IX. Equations (11) and (12) constitute the mathematical basis required for testing. The calculation of tip displacement, and not simply a comparison of strain measurements, is required because the resistive and optical-strain gauges are of different sizes and are mounted in different locations on the tested cantilevered beam. The next section details the construction of a suitable fiber probe that will function as the measurement arm of the heterodyne interferometer.

Table 144.IX: Table of constants in Eqs. (11) and (12). Geometry was measured with a digital micrometer.

c	1.625 mm
L	260 mm
x_1	51.5 mm
x_2	200.2 mm
x_3	7 mm
η	1.515
p_{e}	0.284

Probe Design

Encompassing the measurement arm of a heterodyne interferometer in SM optical fiber provides the advantages of high resolution and range in the metrology system, customizable probes that can be easily replaced with standard fiber connectors, and remote sensing. SM fiber was chosen over other fiber types because its small diameter will least affect the dynamics of the target structure.

The constructed probes consist of a fiber-optic connector/physical contact (FC/PC) connector from Fiber Instrument Sales, Thorlabs SM 600 fiber, and Fiber Instrument Sales SM fiber ferrules. The fiber is stripped of the acrylic coating and epoxied into the FC/PC connector, which is ground and polished once the epoxy has had ample time to dry. The other end of the fiber probe is then stripped and epoxied into a bare FC/PC fiber ferrule. Again, once the epoxy has had ample time to dry, the ferrule is ground and polished to obtain an optically flat surface. The bare ferrule end of the probe is then coated with a reflective material; sputter-coated gold, platinum, and evaporative-coated aluminum have all been used. The reflective coating provides a measurement signal in the interferometer for this application, although alternative setups are also possible to measure the transmitted signal through a strained portion of fiber.

Multiple probes were constructed, although it was difficult to polish bare FC/PC fiber ferrules, resulting in low power-measurement signals. A few satisfactory probes were constructed, however, and subsequently mounted to an aluminum ruler for testing. A fiber-contained interferometer was then constructed to measure the OPL change in the fiber strain probe as it is strained. A sample fiber strain probe can be seen in Fig. 144.25.

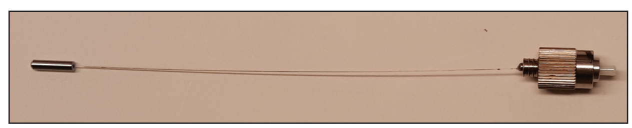

G10694JR

Figure 144.25
A sample single-mode (SM) fiber strain probe. The fiber-optic connector/physical contact (FC/PC) connector can be seen on the right and an aluminum-coated ferrule on the left.

Interferometer Design

A fiber-contained heterodyne interferometer has been designed to interface with an optical-strain probe that functions as the measurement arm of the interferometer. The optical design is based on the free-space heterodyne interferometer designed by Gillmer,[7] which obtained a resolution of the order of 1 to 5 nm. The heterodyne interferometer was chosen over other options, such as a homodyne interferometer, because of the relative power insensitivity of phase measurements and the ability to resolve displacement direction.

A fiber-optic interferometer minimizes alignment time and effort and allows for a compact, flexible design; a schematic of the optical design is seen in Fig. 144.26. Instead of beam splitters in free space, two 2 × 2 polarization-maintaining (PM) fiber-optic couplers were used. As seen in Fig. 144.26, a Thorlabs HRS0145 frequency-stabilized HeNe laser passes through a free-space beam-splitting cube; each beam then passes through an Isomet acousto-optic modulator (AOM). The first-order beams are selected from each AOM, imparting a frequency shift of 80 MHz and 80.07 MHz to create a 70-kHz split frequency between the measurement and reference beams. The 70-kHz split frequency was chosen based on the bandwidth of the lock-in amplifiers (LIA's) used in testing. The two beams are then launched into the PM fiber couplers with Thorlabs PAF-X-5-B fiber launchers. The reference arm of the interferometer is created by putting one FC/PC output of one coupler into optical contact with a plane mirror. The measurement arm of the interferometer is created by connecting the SM fiber probe to the PM coupler. Two photodiodes are used to acquire the measurement and reference signals, which are passed to a Stanford Research Systems SR830 LIA. The phase shift and power from the output of the LIA are calculated as

$$P = \sqrt{X^2 + Y^2}, \tag{13}$$

$$\phi = \tan^{-1}\left(\frac{Y}{X}\right), \tag{14}$$

where P is the measurement signal power and ϕ is the phase shift between the reference and measurement signals wrapped from $-\pi/2$ to $\pi/2$. The phase is then unwrapped with Matlab and used with Eq. (10) to calculate the tip displacement of a cantilevered beam. The X and Y outputs of the LIA were recorded with an NI CDaQ 9174 with an NI 9125 voltage module installed; an NI 9325 strain module was used to record a resistive-strain gauge signal for reference.

The stability of the interferometer was assessed by removing the SM probe from the measurement arm and, instead, putting the coupler fiber connector in optical contact with a plane mirror. The OPL difference between the two arms of the interferometer over a 30-s time interval is seen in Fig. 144.27. The test shows that there is drift of the order of 70 nm within the interferometer itself, even with passive environmental isolation, which limits the resolution of current measurements. Even with this limitation, testing continued to measure the displacement of a cantilevered beam. It is important to note that the interferometric phase measurement does not measure an absolute position but rather a displacement from an assumed reference point.

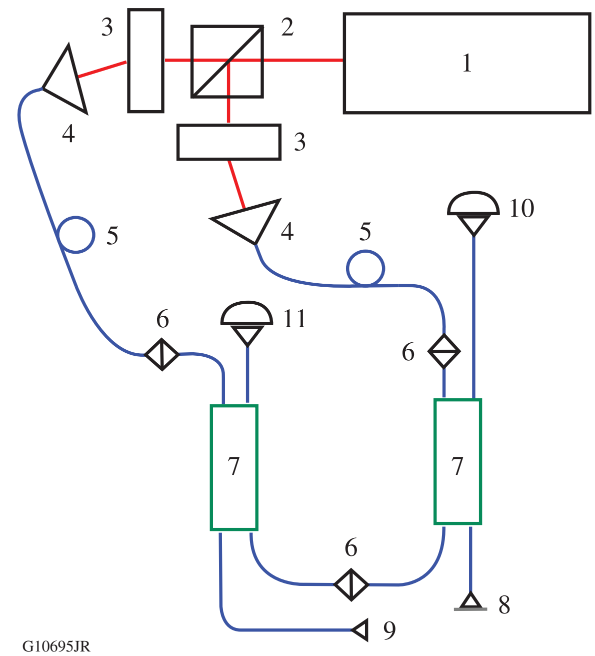

Figure 144.26
Schematic of the optical design of the fiber-contained heterodyne interferometer: (1) frequency-stabilized HeNe laser; (2) nonpolarizing beam splitter; (3) acousto-optic modulator; (4) fiber launcher; (5) polarization-maintaining (PM) patch cable; (6) FC/PC-to-FC/PC connector; (7) 2 × 2 PM fiber coupler; (8) plano mirror reference; (9) to measurement arm/probe; (10) reference photodiode; and (11) measurement photodiode.

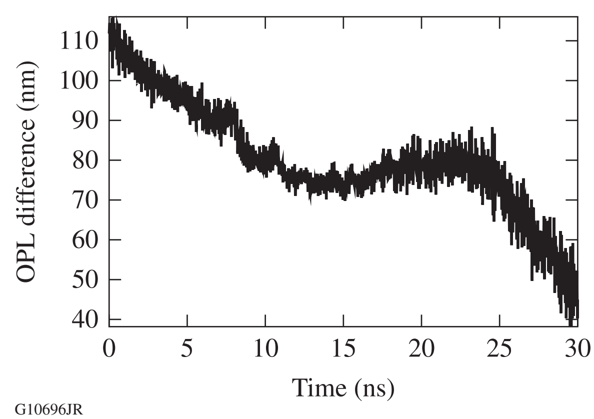

Figure 144.27
A stability test of the fiber-contained interferometer measuring the optical-path–length (OPL) difference between two fixed arms of the heterodyne interferometer.

1. Strain Measurements

Strain measurements were taken using a cantilevered aluminum beam substrate (260 mm × 25.4 mm × 3 mm) with the SM fiber strain probe and heterodyne interferometer, along with a resistive-strain gauge for reference. The voltage data from the LIA and measurements by the resistive-strain gauge were both recorded with the NI CDaQ 9174. A static measurement (Fig. 144.28) was taken while the end of the test cantilever was held in place. The static resistive-strain gauge measurement has significant high-frequency noise, whereas the optical measurement is subject to low-frequency noise and measurement drift. The low-frequency noise in the optical measurement could be caused by higher-order bending modes of the pinned beam, which are not taken into account by Eq. (11). Static measurements show that the noise floor of the optical-strain gauge is below that of the resistive-strain gauge used here.

Two quasi-static tests, each obtained by displacing the tip of the substrate cantilever with 90° rotations of a 1/4–20 unified national coarse (UNC) screw, are seen in Fig. 144.29 with offsets for clarity; the total displacement of each test was nominally 1.27 mm. The measured displacements calculated

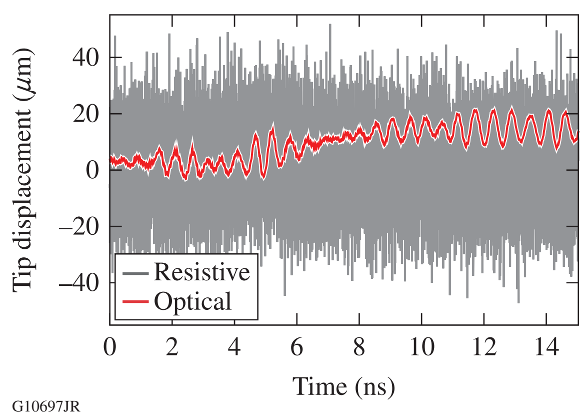

Figure 144.28
Strain measurements of a statically held cantilever. The noise floor is significantly higher for the resistive-strain gauge than for the optical-strain gauge.

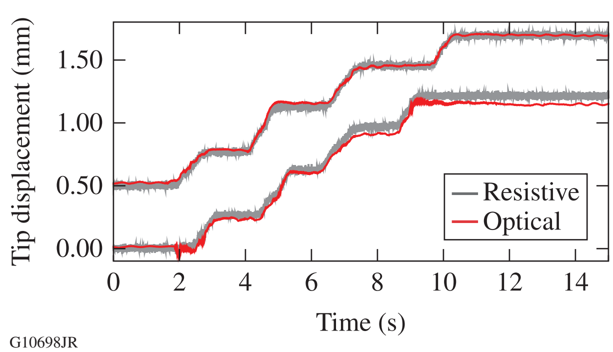

Figure 144.29
Calculated tip displacements from measured optical probe and resistive-strain gauge strains from a fiber-contained heterodyne interferometer when the beam tip is displaced with a 1/4–20 screw in $\pi/2$ increments. The data for each of the tests are offset for clarity.

from the resistive- and optical-strain measurements agree on the whole, although the optical measurements may be subject to dynamic effects seen in the bottom plot in Fig. 144.29. If the two calculated tip displacements are plotted against each other (Fig. 144.30) with a linear fit, a clear linear relationship is observed between the two displacements. The noise of this comparison is again governed by the noise of the resistive-strain gauge. The error from the linear fit in Fig. 144.30 is seen in Fig. 144.31.

Dynamic testing was completed by impulse loading the free end of the cantilevered beam. When pinged, the beam-tip calculations should show harmonic decay as the canitlever is left free to vibrate. The calculated resistive-strain gauge tip

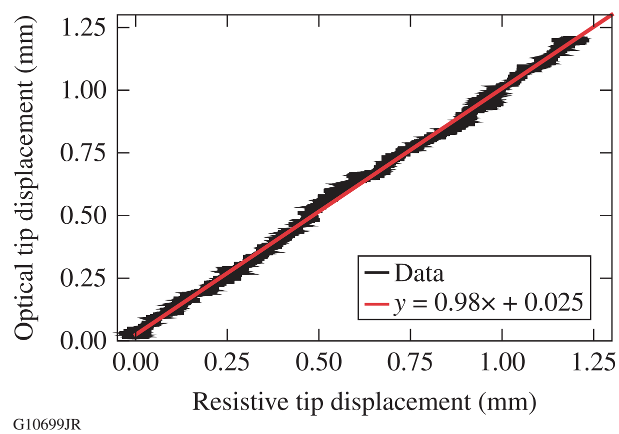

Figure 144.30
Calculated optical and resistive-tip displacement when the beam tip is displaced with a 1/4–20 screw.

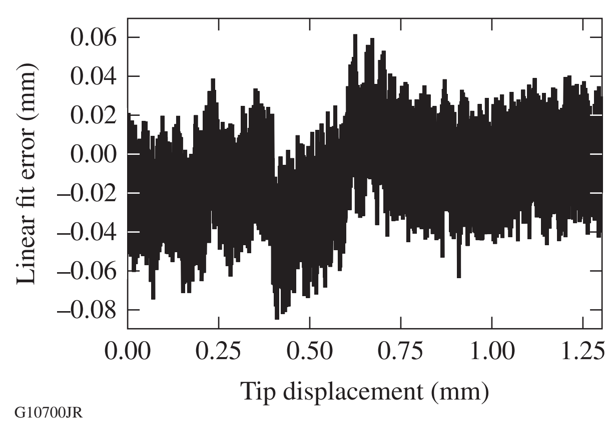

Figure 144.31
Calculated tip-displacement error between optical-probe and resistive-strain gauge measurements from a fiber-contained heterodyne interferometer when the beam tip is displaced with a 1/4–20 screw.

displacement of a dynamic measurement (Fig. 144.32) clearly exhibits the expected harmonic decay; however, the optical measurement encounters a difficulty with dynamic measurements. The power and phase measurements from the LIA, seen in Figs. 144.33 and 144.34, respectively, do not clearly exhibit harmonic decay. The power of the optical measurement signal approaches zero at a number of points in the dynamic test, resulting in phase jumps. In practice, this would mean the location of the target would be lost and any closed-loop stabilization system would fail.

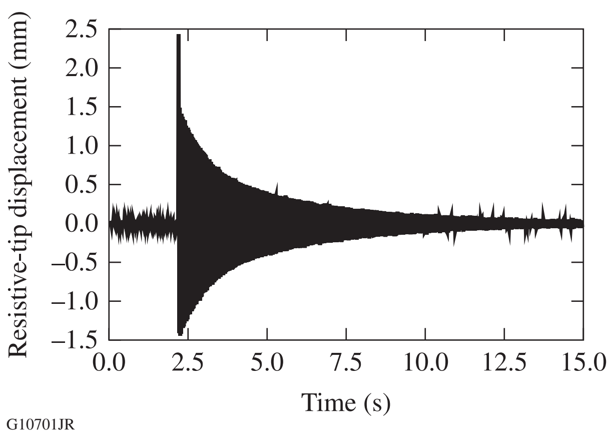

Figure 144.32
Calculated resistive-strain gauge tip displacement of a dynamic test. Harmonic decay can be clearly observed.

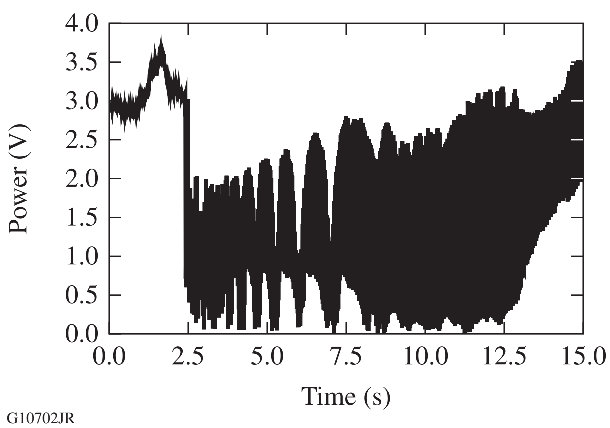

Figure 144.33
Power of the lock-in-amplifier's (LIA's) measurement signal for the optical metrology system of a dynamic test. The measurement power approaching zero results in a loss of measurement signal.

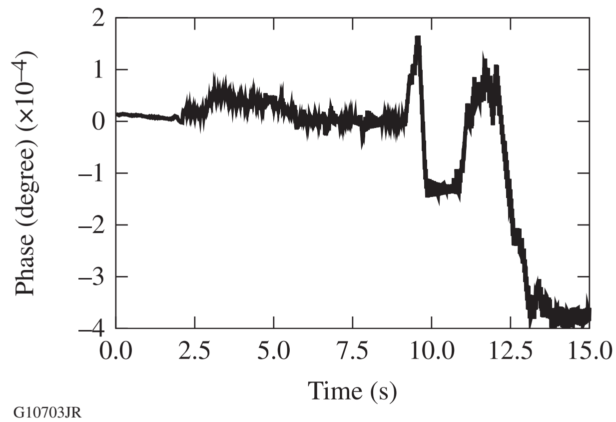

Figure 144.34
Phase of the LIA measurement signal for the optical metrology system of a dynamic test. Phase jumps are seen whenever the power in Fig. 144.33 approaches zero.

Discussion

Calculated tip displacements in Fig. 144.34 show that the optical-strain gauge measurements agree with the reference resistive-strain gauge values for semi-static experiments. The assumption in Eq. (11) that there is no temperature drift may be responsible for some of the measurement error; shorter time-scale testing could mitigate temperature drift. There are two primary sources of error in the interferometer: environmental drift within the interferometer and error seen in testing. Environmental temperature variations and vibrations can be mitigated by minimizing the length of fiber in the interferometer and by instituting improved environmental isolation for both the interferometer and experimental setup. The error seen in testing (Fig. 144.31) is largely governed by the noise in the resistive-strain gauge; however, qualitative evidence implies that there is a dynamic effect in which the strain rate affects the measurement and/or that the constants seen in Table 144.IX are incorrect. Dynamic measurements with the optical sensor were not successful because of measurement-signal power loss. As the sensor is displaced, stress birefringence in the fiber could modify the polarization state of the light. As the polarization state in the measurement arm is varied and the reference arm polarization state kept relatively constant, two orthogonal polarization states could be present, resulting in the absence of an interference signal and causing the measurement power loss and phase jumps. Measurements with a polarimeter show that the polarization state of the light is significantly varied after passing through the fiber probe, lending credence to this explanation for the measurement power loss in dynamic measurements. The failure of the sensor in dynamic measurements precludes its use for target position metrology at this time, although other applications for the sensor such as high-resolution, semi-static strain monitoring at cryogenic temperatures exist.

The main advantage of the optical sensor is the higher resolution when compared to the resistive-strain gauge used here. Common strain gauges routinely obtain resolutions of $\approx 2\ \mu\epsilon$ (peak to peak), which is equivalent to 28 μm of tip displacement in this experiment. The resolution of the optical-strain gauge is limited by the phase measurement of the LIA, which has a stated resolution of 0.01°—equivalent to a 54.5-nϵ resolution limit of the optical-strain gauge with this test geometry. In practice, the resolution of the optical-strain gauge is worse because of the environmental effects, namely the drift seen in Fig. 144.27, although the resolution of the fiber probe sensor is $\approx 0.8\ \mu\epsilon$ (peak to peak), or 11 μm of tip displacement in this experiment, which will substantially increase with environmental isolation. The heterodyne application does not lend itself to easy multiplexing because of the drastic increase in required source power and additional optics detectors. Essentially, for each sensor, the fiber-contained interferometer must be copied and the source power increased. Although the optical design allows for remote sensing, any temperature changes, strains, or vibrations along the entire measurement path will be measured as a phase change. Great care must be taken to ensure that only the area of interest is under measurement. One method to ensure this is to create a differential measurement system with a second fiber-based sensor that measures the OPL change up to the area of interest (i.e., two interferometric strain measurements).

Future Work

Minimizing the lengths of fiber in the interferometer requires custom-made components that cannot be fabricated onsite. Improved environmental control will be implemented for further testing to minimize environmental drift in the interferometer. Further stress-optic modeling and dynamic testing of the strain probe are required for dynamic applications.

Conclusion

A new optical-based strain metrology system consisting of a SM fiber strain probe and a fiber-contained heterodyne interferometer has been discussed. A resolution limit of 54.5 nϵ has been shown for the optical-strain gauge, compared to 2000 nϵ for a common resistive-strain gauge. A governing theory for the conversion of an optical phase change to the displacement of the tip of a cantilevered beam has been derived. Successful static and quasi-static experimental results have been presented and the operation of the metrology system discussed. Drift in the interferometer, attributed to long fiber lengths and ambient environment fluctuations, limited the resolution of the optical measurements. Dynamic measurements were unsuccessful because of measurement signal power loss, precluding the use of the system for target position metrology without further work. The strain sensor described here is an alternative to established strain metrology methods for demanding and extreme environments, such as cryogenic environments at LLE, for specific applications.

ACKNOWLEDGMENT

This material is based upon work supported by the Department of Energy National Nuclear Security Administration under Award Number DE-NA0001944, the University of Rochester, and the New York State Energy Research and Development Authority. The support of DOE does not constitute an endorsement by DOE of the views expressed in this article.

REFERENCES

1. J. J. Dosch *et al*., J. Intell. Mater. Syst. Struct. **3**, 166 (1992).
2. I. Latka *et al*., Cryogenics **49**, 490 (2009).
3. X. Dong, H. Y. Tam, and P. Shum, Appl. Phys. Lett. **90**, 151113 (2007).
4. C. D. Butter and G. B. Hocker, Appl. Opt. **17**, 2867 (1978).
5. A. Othonos, Rev. Sci. Instrum. **68**, 4309 (1997).
6. J. D. Ellis, *Field Guide to Displacement Measuring Interferometry*, Vol. FG30 (SPIE Press, Bellingham, WA, 2014).
7. S. R. Gillmer, "Development of a Novel Fiber-Coupled Three Degree-of-Freedom Displacement Interferometer," M.S. thesis, University of Rochester, 2013.